Journal of Manufacturing Processes 50 (2020) 467–474

Contents lists available at ScienceDirect

Journal of Manufacturing Processes

journal homepage: www.elsevier.com/locate/manpro

Tapered mask and its effect on the fluid flow and machining efficiency of a multiphase jet

Yan Hu, Qingwen Dai, Wei Huang, Xiaolei Wang*

National Key Laboratory of Science and Technology on Helicopter Transmission, Nanjing University of Aeronautics & Astronautics, Nanjing 210016, China

ARTICLE INFO

Keywords:
Multiphase jet
Tapered mask
Stagnation effect
Machining efficiency

ABSTRACT

Multiphase jet machining (MJM) is a novel surface texturing technique that accelerates the mixture of abrasives and water by compressed air for removal of materials. Here, the significant stagnation effect of masked MJM was reported for the first time; this effect can yield a much lower machining efficiency than the masked abrasive air jet machining and unmasked MJM. It was found that using masks with smaller taper angles improves the machining efficiency and the sidewall slope of the channel. Moreover, reducing the jet angle also elevates the efficiency. Machining mechanisms were revealed and described in terms of the slurry pressure and flow velocity in the stagnation zone. Overall, to improve the machining efficiency of masked MJM, two optimized process parameters were suggested and verified: 1) masks with a taper angle of 30° or smaller; 2) nozzles with an inclined jet angle of 80°.

Introduction

Mechanical seals are widely used in rotating machinery to avoid leakage between dynamic and static rings. The wear on the mating surface is a serious problem that limits the stability and durability under the condition of high temperature, high pressure and high speed [1]. In recent years, surface textures such as microchannels or dimples have been proven to be an effective approach for ameliorating the tribological and sealing properties of mechanical seals [2–4].

Many materials used for mechanical seals, including cemented carbide and silicon carbide, are hard and brittle materials that are difficult to machine. Current process techniques for micromachining such as laser machining [5,6], micromilling [7] and dry or wet etching [8] are inevitably associated with either a high processing cost, low precision of the machining profile, or microcracking caused by either the processing force or heat. Multiphase jet machining (MJM) is a newly developed technique for the fabrication of surface textures on the mating face of mechanical seals that is promising due to its distinct features of the absence of a heat-affected zone (HAZ) and a high etching rate for brittle materials [9,10]. The inset of Fig. 1 shows the formation mechanism of a multiphase jet. Briefly, when compressed air passes through the nozzle at high speed, the mixture of the abrasive and water is drawn into the mixing chamber by the negative pressure created in the nozzle and then mixes with the air to accelerate the formed multiphase jet that flows to the substrate of the workpiece. Abrasive water jet machining (AWJM), abrasive air jet machining (AAJM) and abrasive slurry jet machining (ASJM) are similar or original processing methods. Table 1 shows the features and working conditions of these methods reported in the literature. As shown in Table 1, AAJM can achieve high-speed flow using inexpensive air pumps with low pressure; nevertheless, it faces significant problems with dust pollution and abrasive recycling. AWJM usually requires the use of expensive high-pressure water pumps, and because of its high kinetic energy, it is always associated with poor machining quality and is primarily used for cutting. ASJM pumps the premixed slurry at a pressure higher than that used in AAJM, and its jet flow velocity is much lower than that of AAJM. In fact, MJM uses an inexpensive air pump, and the used Laval nozzle can obtain a supersonic air fluid at the pressures less than 0.6 MPa. Compared with AWJM and AAJM, MJM can not only achieve the same jet flow velocity under a much lower pressure than that in AWJM but also solve the problems of high cost and environmental pollution commonly found in AAJM [9].

In various types of abrasive jet machining, the stagnation effect is a phenomenon of the fluid flow velocity in the Z-axial direction falling rapidly to zero after the jet approaches the workpiece. Parameters such as the size of the processing area [14], the jet angle and the microtexture shape will all influence the stagnation effect.

In the MJM process, an erosion-resistant mask that tightly adheres or is magnetically attracted to the surface of the target material is needed for the desired features and dimensions. Clearly, thick masks

* Corresponding author at: Yudao street 29#, Nanjing, China.
E-mail address: wxl@nuaa.edu.cn (X. Wang).

https://doi.org/10.1016/j.jmapro.2020.01.006
Received 30 July 2019; Received in revised form 31 December 2019; Accepted 4 January 2020

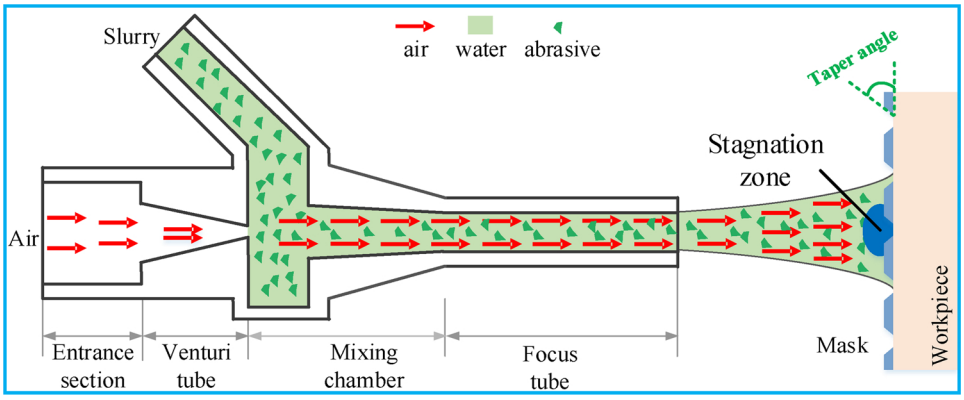

Fig. 1. Micromachining in multiphase jet machining (MJM).

Table 1
Literature results for the AAJM, ASJM and AWJM jet pressure and velocity.

Types	Jet pressure (MPa)	Jet velocity (m/s)	Driving modes	Methods
AAJM		120–150 [11]	Air pressure (0.43–0.69 MPa)	Calculation and measurement
		150–200 [12]	Air pressure (0.2 MPa)	Simulation
		100–200 [13]	Air pressure (0.1–0.3 MPa)	Measurement
ASJM	2–4 [14]	49–127	Water pressure (1.2–8 MPa)	Simulation
		42–89 [15]	Water pressure (2–4 MPa)	Calculation
AWJM		40–160 [16]	Water pressure or velocity (35 MPa, 180 m/s)	Simulation
	40–100 [17]	250–450	Water pressure (100 MPa)	Simulation

Table 2
Physical properties of SD, RBSC, and SUS304.

Materials	Density ρ,g/cm^3	Hardness	Elasticity modulus *E*, GPa	Tensile strength σ_b, MPa
SD	3.52	HV 1000	1100	1050-3000
RBSC	3.05	HRA 91	330	352
SUS304	7.93	HRB 89	193	535

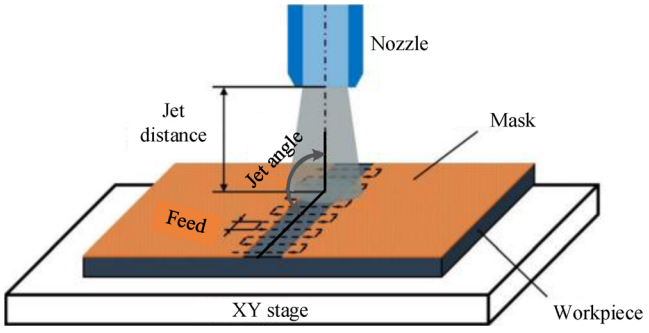

Fig. 2. Schematic diagram of the S-type feeding mode.

can be reused because of their high erosion resistance. Previously, numerous researchers have tried to use thick masks in the abrasive jet machining to obtain various dimensional microstructures with high precision [18–21]. Ghobeity et al. [22] found that the definition of straight channel edges on glass plates is improved significantly by using the thick steel masks.

When the accelerated abrasive particles reach the stagnation zone, the particle behaviors such as collisions and rebounds may make the process rather complex. In particular, the additional thick masks can change the flow characteristics around the impinging particles and the workpiece, including properties such as the jet flow pressure, particle flow velocity, fluid flow direction, and the degree of particle bottom and wall rebound, thereby inevitably affecting the machining efficiency, profile and quality. For the texture profile, the “blast lag” effect is an example of this influence, where the narrow-mask [23] and thick-mask [21] jet machining more rapidly develop sloped sidewalls that meet in the center to form a V-shape and obtain a large centerline depth. On the other hand, for impact velocity, Dehnadfar et al. [24] found that the particle velocities of AAJM through a narrow mask opening were clearly lower than that in the free jet, thus lowering the erosion rate of the narrow masked channels, as shown by Haghbin [19]. Kowsari et al. found that the stagnation zone in a deeper channel was larger than that in a shallower channel, thus having smaller impact velocities and producing lesser erosion in deeper channels [14]. In other words, such small impact velocity and erosion will also occur in the thick-mask jet machining.

Compared to AAJM (only air), MJM is more complicated because of the coexistence of air and water. The stagnation of MJM and its severity remain unclear. It may be significant because the density and viscosity of water are approximately 700 and 100 times greater than those of air. Additionally, the development of an effective method for enhancing the machining efficiency of MJM with narrow or thick-masks and maintaining the desired feature is a technical challenge that should be investigated. More importantly, to date, studies on masks mainly focus on their thickness and width [19]. It is currently unknown whether it is possible to improve the processing performance by changing the shape of the mask, particularly for the MJM process.

Herein, this study for the first time provides a comprehensive understanding of the machining differences between MJM and AAJM. Then, thick masks were used in this work to obtain a good machining boundary. The tapered masks of SUS304 with different angles were designed to ameliorate the abovementioned dilemmas. On the basis of mask shape optimization, the machining effect of the jet impact angle was also investigated.

Experimental design

Machining details

A reaction-bonded silicon carbide (RBSC) ring, which is a hard and brittle material typically used in the mechanical seals, was chosen as the test material. Because of its high hardness compared with silicon carbide, synthetic diamond (SD) with a particle size of 13 μm was selected as the microabrasive. Due to its good resistance in erosion and

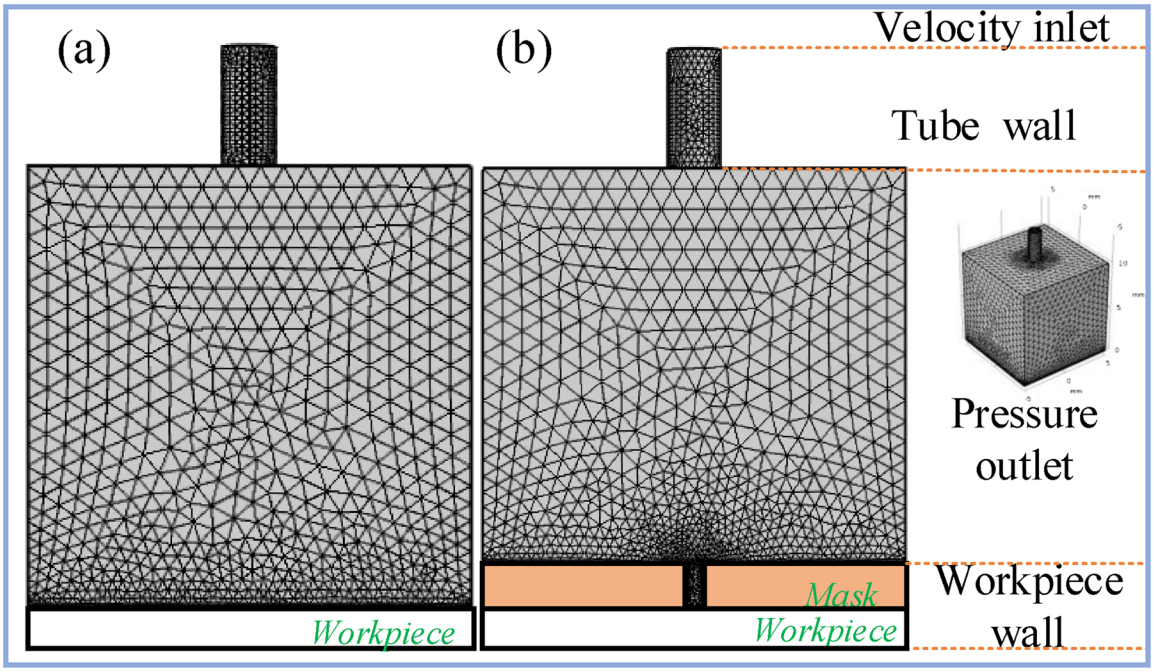

Fig. 3. 3D modeling of (a) unmasked jet and (b) masked jet machining.

Table 3
Parameters for 3D modeling of unmasked and masked jet machining.

Inlet velocity	200 m/s
Outlet pressure	0 Pa
Reference pressure	101325 Pa
Focus tube diameter	1.6 mm
Mask thickness	3 mm [22]
Mask opening width	500 μm
Mask taper angle	30, 60, 90°

machining properties, SUS304 was used as the mask material. The main material properties of reaction-bonded silicon carbide, synthetic diamond, and SUS304 are listed in Table 2.

According to the calculations of Li et al. [11] and the experimental data of Su et al. [[9]], the maximum machining efficiency of MJM can be obtained at the jet distance of 10 mm. Hence, this distance was chosen in both the simulation and experiments performed in this study. Two scanning modes were studied, including the fixed jet mode and the S-type feeding mode shown in Fig. 2. In the fixed jet mode, the nozzle

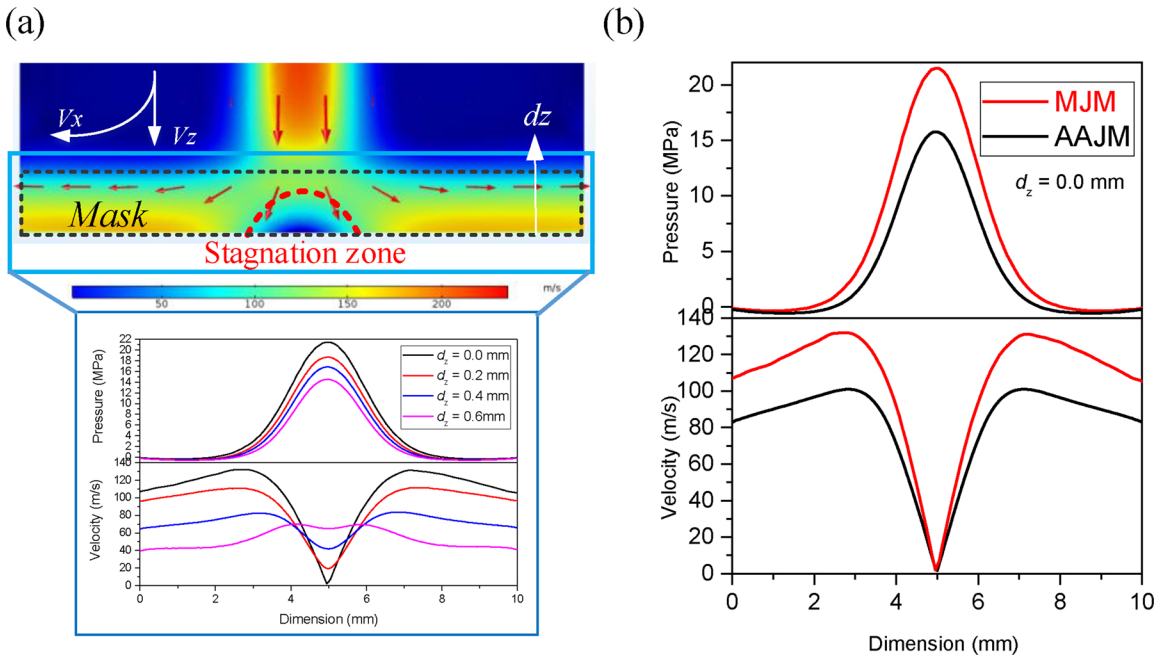

Fig. 4. (a) Pressure and velocity distribution in the vicinity of the stagnation zone as obtained by simulation and (b) their comparison between the masked MJM and AAJM.

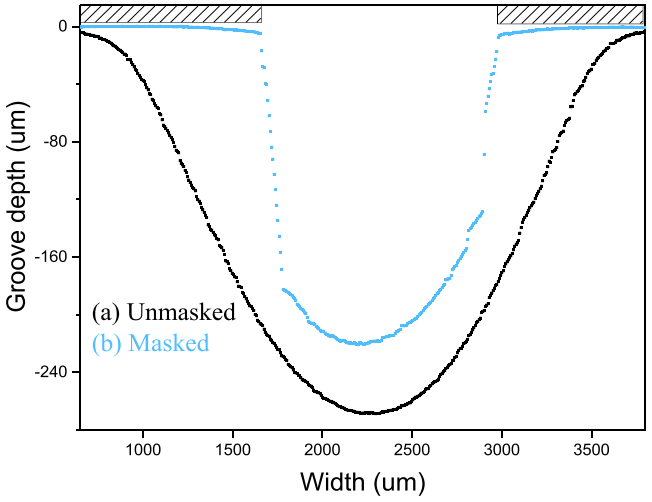

Fig. 5. Groove profiles machined by (a) unmasked and (b) masked MJM.

was fixed at the height of 10 mm from the workpiece. The S-type feeding mode was realized by moving the workpiece along the groove direction and synchronously oscillating the workpiece relative to the nozzle in the direction perpendicular to the mask edge. In S-type feeding mode, the feed rate is 100 μm, and the nozzle scan velocity is 0.2 mm/s.

The processing-related details of the structures were observed by a 3D optical profilometer (Bruker, USA). The surface roughness was measured by the 3D optical profilometer on a rectangle area of 30 μm × 37 μm on the groove bottom.

Simulation modeling

To obtain the jet velocity and pressure distribution in the stagnation zone, a series of simulations were performed in this study using the COMSOL Multiphysics fluid dynamics software (COMSOL Inc., Sweden). In this software, the standard k-ε model can be used to describe both compressible and incompressible turbulent flow, as was reported in many previous studies [14,16,17]. Unlike the AWJM, the air driving jet in the MJM and AAJM process is a compressible turbulent flow, such that the weakly compressible flows in the simple standard k-ε model were chosen for the calculation. The standard formulas of the k- < epsilon > model and level set are used in the mixture flow mode as below:

$$\rho(u\cdot\nabla)k = \nabla\cdot\left[(\mu + \frac{\mu_T}{\sigma_k})\nabla k\right] + P_k - \rho\varepsilon$$

$$\rho(u\cdot\nabla)\varepsilon = \nabla\cdot\left[(\mu + \frac{\mu_T}{\sigma_\varepsilon})\nabla\varepsilon\right] + C_{\varepsilon 1}\frac{\varepsilon}{k} - C_{\varepsilon 2}\rho\frac{\varepsilon^2}{k}$$

$$\mu_T = \rho C_\mu \frac{k^2}{\varepsilon}$$

$$P_k = \mu_T\left[\nabla u/(\nabla u + (\nabla u)^T) - \frac{2}{3}(\nabla\cdot u)^2\right] - \frac{2}{3}\rho k\nabla\cdot u \quad (1)$$

$$\frac{\partial\phi}{\partial t} + \nabla\cdot(u\phi) = \gamma\nabla\cdot(\varepsilon_{ls}\nabla\phi - \phi(1-\phi)\frac{\nabla\phi}{|\nabla\phi|}) \quad (2)$$

where ρ and μ denote the fluid density and viscosity, k is the turbulence kinetic energy, and ε is the turbulent dissipation rate. u is the fluid velocity and φ changes from 0 to 1. For the compressible fluid, the turbulence correlation constants are given as $C_{\varepsilon 1}$ = 1.44, $C_{\varepsilon 2}$ = 1.92, C_μ = 0.09, σ_k = 1.0, and σ_ε = 1.3. The values for the initialization γ and interface thickness ε_{ls} are 140 m/s and 6.5e-4 m, respectively.

Fig. 3 shows the 3D geometrical modeling of the unmasked and masked jet machining. All unstructured meshes with an average unit-quality between 0.93 and 0.98 were automatically generated by the COMSOL software. Clearly, compared with AAJM, the addition of water increases the density and viscosity of the multiphase jet. After measuring the mass and volume flow rate of the fluid passing through the nozzle over a certain period of time, the average densities of the abrasive air and multiphase jet were calculated to be 1200 kg/m^3 and 1500 kg/m^3, respectively. The viscosity of the AAJM mixture is equal to the air viscosity (0.001 Pa s), the viscosity of MJM is equal to the water viscosity (0.1 Pa s), and the compressibility coefficient is 1. In the simulation, the walls of the workpiece and the focus tube are considered

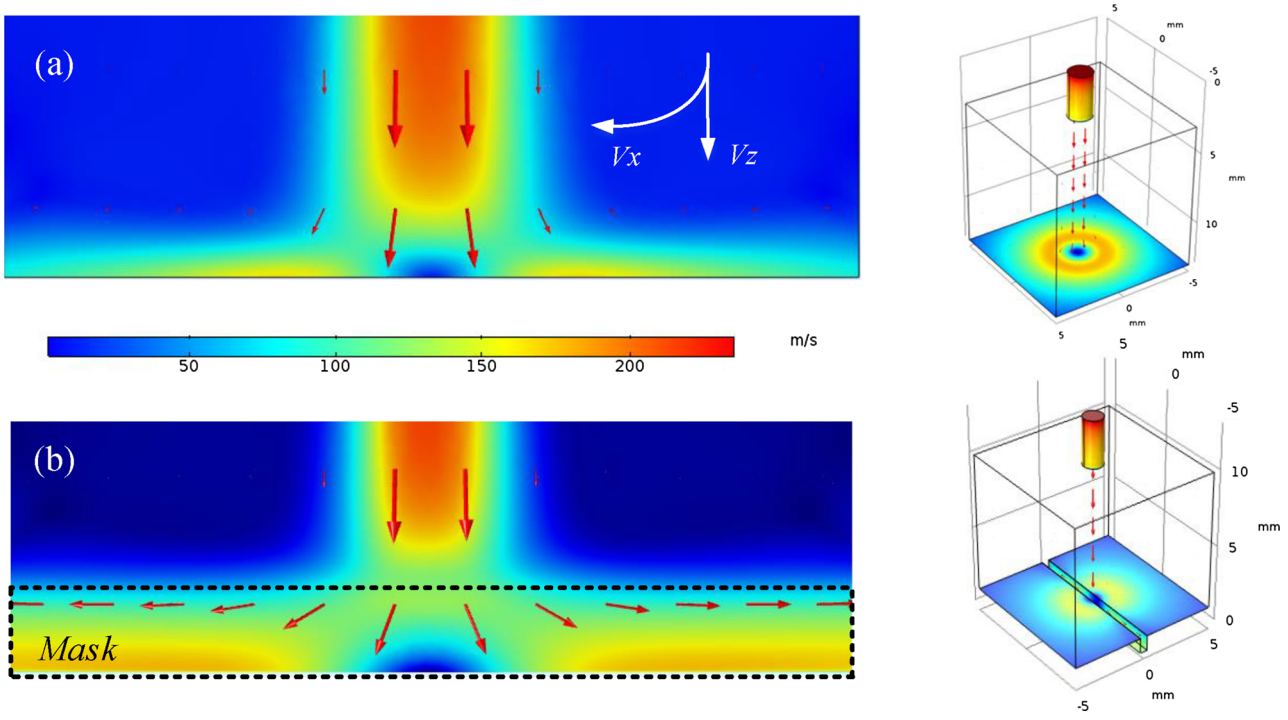

Fig. 6. Effects of (a) unmasked and (b) masked MJM on the slurry velocity contours obtained by simulation.

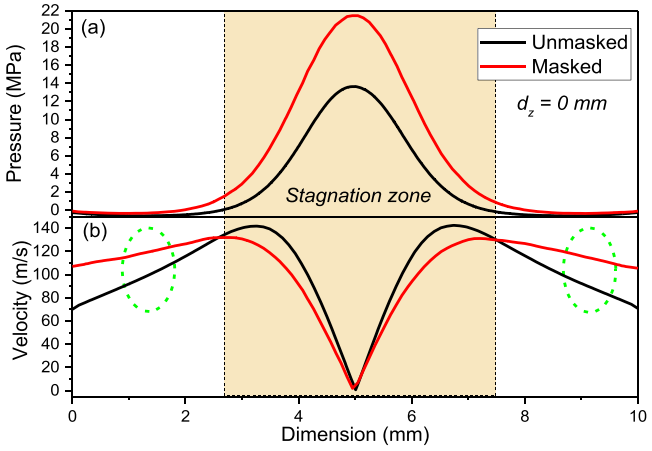

Fig. 7. (a) Pressure and (b) velocity distribution in the vicinity of stagnation zone obtained by simulation.

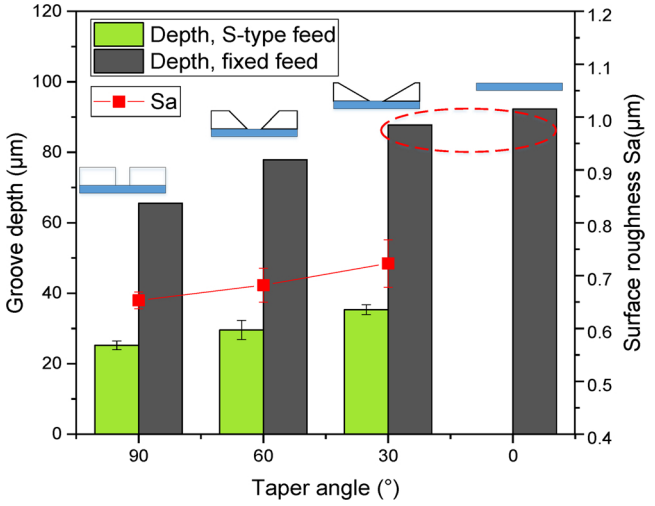

Fig. 8. Effect of the mask taper angle on the groove depth and surface roughness.

to be rigid walls without slip. It is assumed that the model is initially filled with air and no slip exits among the three phases in this model. The boundary conditions of the solver are set as shown in Table 3.

Results and discussions

Stagnation effect in masked AAJM and MJM

Taking the masked MJM as an example, when the jet impacts on the substrate of the workpiece, a high pressure and low velocity zone will exist at the liquid-solid contact interface that is usually known as the stagnation zone. The simulation results of Fig. 4 are obtained using the method described in Section “Simulation modeling”, and the parameters and conditions are shown in Table 3 and Fig. 3(b). Fig. 4(a) shows the jet pressure and velocity distribution in the vicinity of the masked MJM stagnation zone. It is observed that the jet pressure at the jet-center region clearly increases when it approaches the workpiece. In contrast, the vertical flow velocity (*Vz*) falls rapidly to zero in the Z axial direction and the jet even becomes static as it approaches the workpiece. After the jet impacts the surface of the workpiece, the slurry will be restricted to flow along the horizontal direction. As shown in Fig. 4(a), the horizontal velocities (*Vx*) on both sides away from the stagnation zone are relatively high, reaching the values of approximately 40 − 110 m/s. These values are consistent with the results for the same air-driving slurry jet examined in the work of Nouraei et al. [15].

The simulation results presented in Fig. 4(b) show that the masked MJM has a stronger stagnation zone with a higher pressure and a lower *Vz* than those of the masked AAJM. It is difficult for the abrasive particles in the high-pressure zone to reach the surface of the workpiece, which is also known as the air cushion effect in the air jets and the water cushion effect in the water jets, respectively. Numerous studies have indicated that for the abrasive water or slurry jet machining, a large stagnation zone can give rise to a low erosion rate [14,15,19,26]. In AAJM, air and dry abrasives are drawn into the air stream, while for MJM it is a slurry (water and abrasives). Clearly, compared with AAJM, the water in the MJM process causes an increase in the density and viscosity of the whole jet and the depth of the slurry-filled region in the mask opening. Specifically, the density and viscosity of water are approximately 700 and 100 times greater than those of air, respectively. According to the analysis of the above simulation, because of the greater deceleration of the particles in the water stagnation zone and the strong influence of the fluid density and viscosity on flow confinement, a lower machining efficiency will be obtained in the masked MJM.

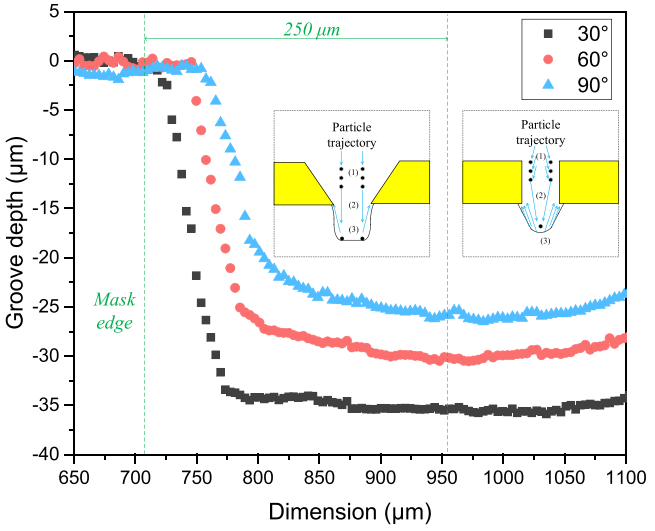

Fig. 9. Effect of the mask taper angle on the channel cross-sectional shapes machined by MJM with the S-type feeding mode.

Stagnation effect in unmasked and masked MJM

The use of masks may change the jet pressure, particle flow velocity, fluid flow direction and other parameters in the stagnation zone, thereby inevitably affecting the machining efficiency, profile and quality. To compare the machining details between the unmasked jet and masked jet machining, two experiments were carried out with a machining time of 10 min, synthetic diamond mass concentration of 10 %, jet pressure of 0.6 MPa and jet angle of 90°. The fixed jet mode was used in this section, and the mask had a thickness of 3 mm and an opening of 500 μm. Fig. 5 shows the cross-sectional profiles of the microfeatures machined by the unmasked and masked MJM. Comparison of the two curves in Fig. 5 shows that the cross-sectional shape and edges of grooves can be well controlled by the mask. The centerline depth of the unmasked groove (268 μm) is 1.07 times that of the masked groove (220 μm), indicating that the erosion rate of the masked MJM is remarkably lower than that of the unmasked MJM.

Fig. 6 shows the velocity distribution images of the unmasked jet and masked jet machining obtained in the simulation. An examination of the color map shows that masked jet machining has a larger stagnation zone than unmasked jet machining. The curves in Fig. 7 are

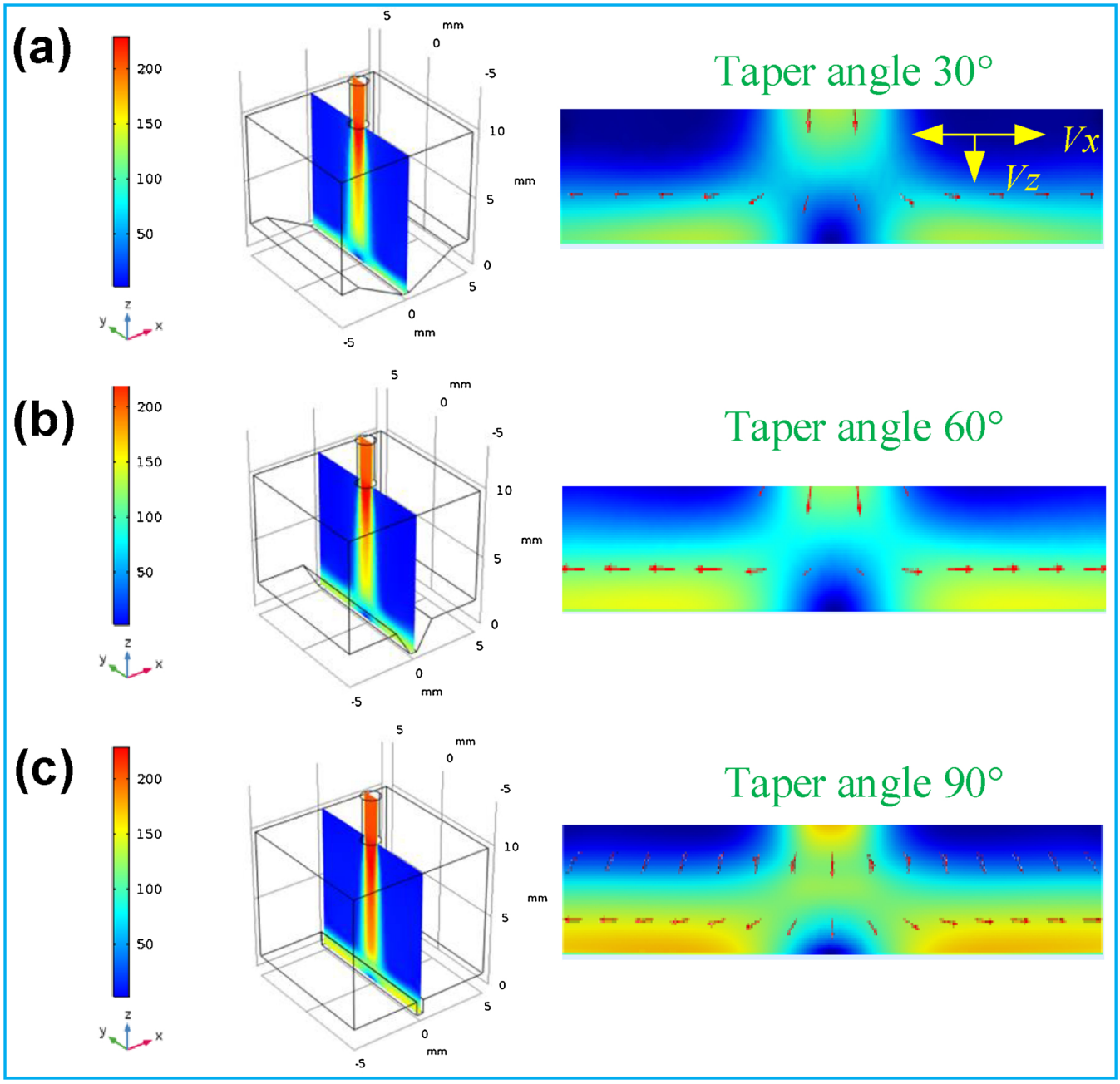

Fig. 10. Velocity contours of the whole flow field for masks with different taper angles obtained by simulation.

obtained from the contact position between the jet and the workpiece (dz = 0 mm). As shown in Fig. 7(a), the pressure of masked jet machining is higher than that of unmasked jet machining, implying that the particle impact velocities Vz are lower for masked jet machining than for unmasked jet machining, thus reducing the machining efficiency of masked jet machining. The velocities Vx in the masked jet (as seen in the green dashed circles of Fig. 7(b)) are higher than those of the unmasked jet, and their role will be discussed in the next section. The use of a mask increases the degree of flow confinement, necessitating the use of some methods for ameliorating the effects of these changes to improve the machining efficiency of masked MJM.

Stagnation effect in masked MJM with different mask taper angles

As shown in Sections "Stagnation effect in masked AAJM and MJM" and "Stagnation effect in unmasked and masked MJM", the masked MJM has a lower machining efficiency than the masked AAJM and the unmasked MJM due to the strong stagnation effect. Three masks with the taper angles of 30°, 60° and 90° were designed to improve the machining efficiency of masked MJM in these experiments. The experiments were conducted at a synthetic diamond mass concentration of 10 %, jet pressure of 0.6 MPa, jet distance of 10 mm and jet angle of 90°. All metal masks have a thickness of 3 mm and an opening of 500 μm, which is convenient for the processing of the tapered opening. In the S-type feed jet machining, the nozzle moving rate is 0.2 mm/s, and the feed rate is 100 μm. In the fixed jet machining, the machining time is 3 min.

Fig. 8 shows the machining groove depths and surface roughness at different mask taper angles, indicating that the mask taper angle has clear effects on the groove depth and roughness. For the S-type feeding mode, with the decrease in the mask taper angle from 90° to 30°, the channel depth increases from 25.22 μm to 35.36 μm, and the surface

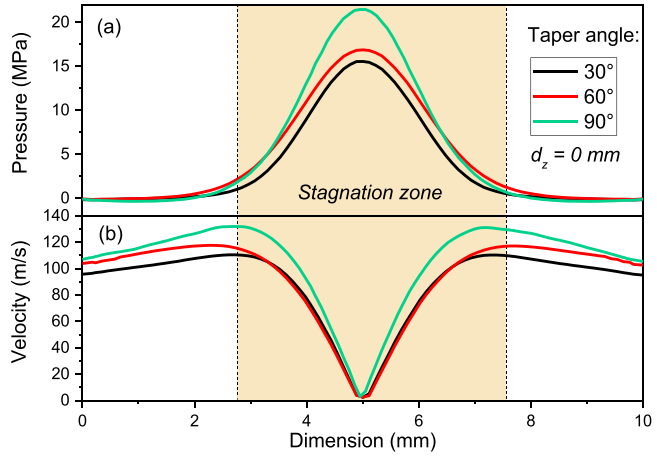

Fig. 11. (a) Pressure and (b) velocity distribution in the vicinity of the stagnation zone obtained by simulation.

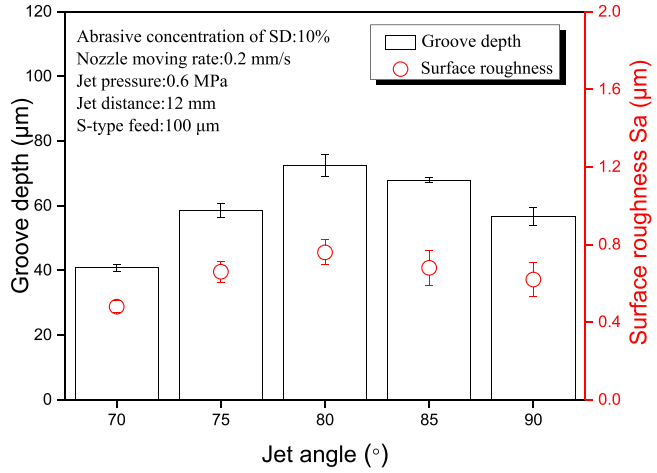

Fig. 12. Effect of the jet angle on the groove depth and surface roughness.

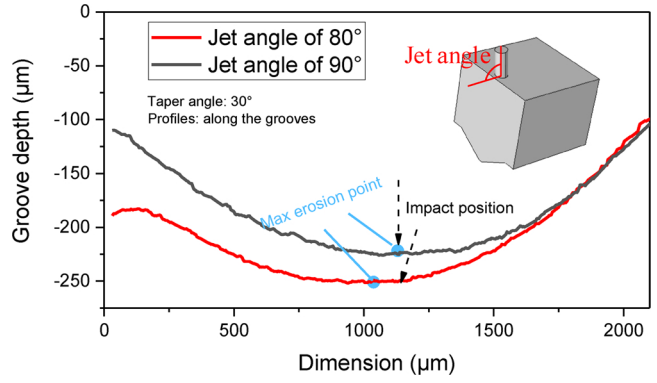

Fig. 13. Machining profiles using MJM with the fixed jet mode and jet angles of 80° and 90°.

roughness of the groove bottom also increases by a factor of 1.1. Therefore, the smaller taper angle improves the machining efficiency, and the machined surface is poor. For the fixed feed mode, the groove depth increases with the decreases in the mask taper angle from 90° to 30°. In particular, as observed in the red dashed circle in Fig. 8, the machining efficiency at the taper angle of 30° is very close to that of unmasked jet machining.

The mask taper angle also has an obvious effect on the machining profile. Fig. 9 shows three channel cross-sectional shapes machined by MJM using the mask taper angles of 30°, 60° and 90° and the S-type feeding mode. The channel with a relatively vertical sidewall at the taper angle of 30° is much flatter than those at the taper angles of 60° and 90°. These machining details indicate that masks with smaller taper angles will reduce the probability of the particle impacting at the center and allow the particles to impact on the substrate almost vertically, significantly increasing the sidewall slope. Consequently, the use of masks with smaller taper angles has the advantage of maintaining the U-shaped channel with a flatter bottom and a more vertical sidewall.

Fig. 10 shows the velocity distribution images of the stagnation zone for the taper angles of 30°, 60° and 90° obtained in the simulations, demonstrating that the taper angle of 90° has the strongest stagnation effect. The curves in Fig. 11 are obtained from the contact position between the slurry and the workpiece ($dz = 0$). A common trend for the stagnation zone is that a high fluid pressure in the stagnation zone corresponds to a low fluid velocity *Vz*. As observed from Fig. 10(a), the pressure is minimum at 30°, which means that the vertical flow speed *Vz* in the stagnation zone is relatively large, thus enhancing the machining efficiency of the 30° taper angle. After the vertical multiphase jet hits the surface of the workpiece, the slurry will be restricted to flow along the horizontal direction of the mask opening length. Figs. 10 and 11 show that the horizontal flow speed *Vx* at the taper angle of 90° is larger than those at the taper angles of 30° and 60°. It is clear that due to the higher *Vx*, the sidewall of the 90° taper angle keeps the slurry flowing fast enough for sufficient surface polishing. Consequently, a larger mask taper angle will achieve a good quality channel with a lower surface roughness.

Stagnation effect in masked MJM with different jet angles

Jet angle is another factor affecting the machining efficiency of MJM. A previous study indicated that the machining efficiency and surface roughness of the 80° jet angle is higher than that of the 90° jet angle for many reasons [18]. One of these reasons may be that the inclined nozzle can provide the horizontal speed of the abrasives, so that the particles have a scratch effect on the surface that can improve the removal efficiency of the material. In addition, the inclined jet makes it easier to disperse the accumulated microabrasive particles and reduce the interaction between the particles, thus reducing the kinetic energy loss of the particles. For the optimized taper angle of 30° and the S-type feeding mode, the experimental results presented in Fig. 12 show the same variation trend of the jet angle as that found in the previous study [18].

Under a 7-min machining time and fixed jet mode, the machining depths of the 80° and 90° jet angles are compared in Fig. 13. It is found that the machining depth of the 80° jet angle is higher than that of the 90° jet angle. The maximum erosion point of the 90° jet angle is consistent with the impact position. When the jet angle is 80°, the maximum erosion point will shift to the vicinity of the impact location (in the direction of the nozzle tilt).

To further illustrate the machining mechanism of the jet angle, the different velocity distributions in the vicinity of the stagnation zone with the jet angles in the 70–90° range were calculated, with the results shown in Fig. 14. The numerically obtained curves presented in Fig. 15 are obtained from $d_Z = 0$ and the direction along the mask opening. It is observed from Figs. 14 and 15(b) that the shape of the stagnation zone and stagnation point is obviously changed by the jet angle. With the decrease in the jet angle, the stagnation points are transferred to the location away from the impact point. As shown in Fig. 15(a), the stagnation pressure first increases and then decreases with the decreased jet angle, and the maximum stagnation pressure is observed near the jet angle of 80°. For the inclined jet machining, the higher stagnation pressure will make the abrasive particles shift to the opposite side and exhibit a higher erosion velocity in the maximum erosion area (see Fig. 15(b)). As shown in Fig. 15(b), in the maximum erosion area, the slurry flow velocity of the 80° jet angle is higher than that of the other jet angles; thus, the machining efficiency of the 80° jet machining is much larger than that of the vertical jet machining.

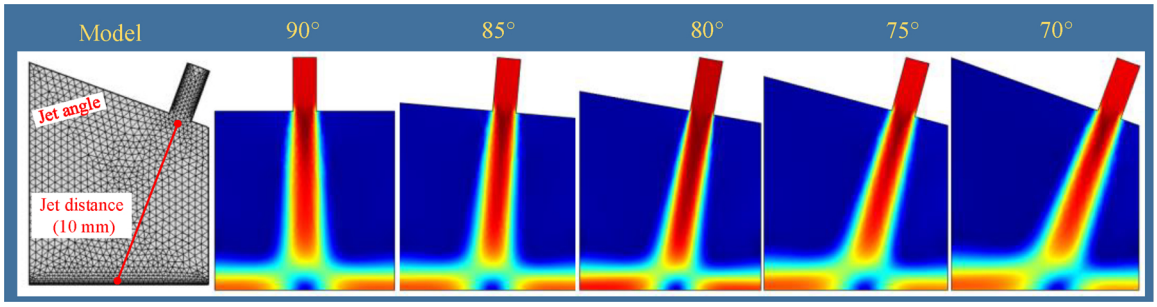

Fig. 14. Velocity contours of the whole flow field for MJM with the jet angles in the 70–90° range obtained by simulation.

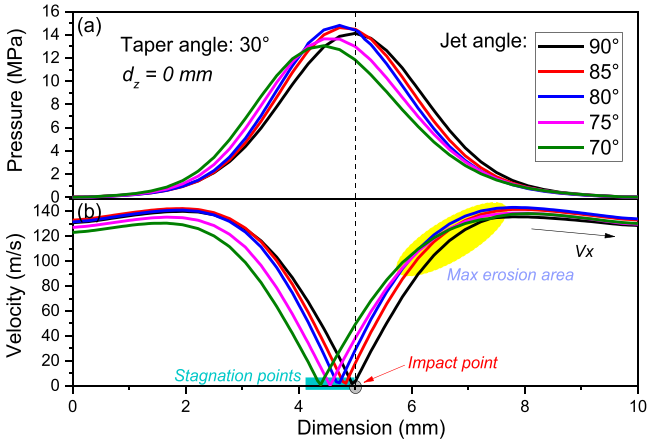

Fig. 15. (a) Pressure and (b) velocity distribution in the vicinity of the static pressure zone obtained by simulation.

Conclusions

Compared to the abrasive air jet machining (AAJM), the existence of water and mask in the MJM process can enhance the stagnation effect, making the machining efficiency of masked MJM far lower than those of the masked AAJM and unmasked MJM. To improve the machining efficiency of masked MJM, a series of experiments were conducted, and the machining process parameters were optimized.

It is found that the use of masks with smaller taper angles decreases the stagnation effect, improving the machining efficiency. The machining efficiency for the taper angle of 30° is very close to that of unmasked MJM. Smaller taper angles can also weaken the “blast lag” effect and have the advantage of maintaining the U-shaped channel with a flat bottom and vertical sidewall.

Compared to the vertical jet machining, inclining the nozzle can improve the machining efficiency to some extent, depending on the inclination angle. The slurry flow velocity of the 80° jet angle in the maximum erosion area is clearly higher than that of the 90° jet angle, resulting in a significant improvement in the machining efficiency.

Declaration of interests

The authors declare that they have no known competing financial interests or personal relationships that could have appeared to influence the work reported in this paper.

Acknowledgments

This work was financially supported by the National Natural Science Foundation of China (Nos. 51675268 and 51805252) and the China Postdoctoral Science Foundation (No. 2019M651822).

References

[1] Etsion I, Michael O. Enhancing sealing and dynamic performance with partially porous mechanical face seals. A S L E Trans 1994;37(4):701–10.
[2] Wang XY, Shi LP, Dai QW, Huang W, Wang XL. Multi-objective optimization on dimple shapes for gas face seals. Tribol Int 2018;123:216–23.
[3] Wang XL, Kato K, Adachi K, Aizawa K. Loads carrying capacity map for the surface texture design of SiC thrust bearing sliding in water. Tribol Int 2003;36(3):189–97.
[4] Shi LP, Wang XY, Su X, Huang W, Wang XL. Comparison of the performances of mechanical gas seals textured with micro-grooves and micro-dimples. J Tribol 2015;138(2):88–90.
[5] Etsion I. State of the art in laser surface texturing. Trans ASME J Tribol 2005;127(1):761–2.
[6] Schreck S, Gahr KHZ. Laser-assisted structuring of ceramic and steel surfaces for improving tribological properties. Appl Surf Sci 2005;247(1):616–22.
[7] Zhang T, Liu ZQ, Xu CH. Influence of size effect on burr formation in micro cutting. Int J Adv Manuf Technol 2013;68(9–12):1911–7.
[8] Wang X, Kato K. Improving the anti-seizure ability of SiC Seal in water with RIE texturing. Tribol Lett 2003;14(4):275–80.
[9] Su X, Shi LP, Huang W, Wang XL. A multi-phase micro-abrasive jet machining technique for the surface texturing of mechanical seals. Int J Adv Manuf Technol 2016;86(5–8):1–8.
[10] Hu Y, Dai QW, Huang W, Wang XL. Accuracy of the pattern transfer from the metal mask to the workpiece surface during multiphase jet machining. Int J Adv Manuf Technol 2019. https://doi.org/10.1007/s00170-019-04607-z. In press.
[11] Li HZ, Wang J, Fan JM. Analysis and modelling of particle velocities in micro-abrasive air jet. Int J Mach Tools Manuf 2009;49(11):850–8.
[12] Luo XY, Palumbo J, Papini M, Spelt JK. Aerodynamic focusing of an abrasive air jet and its effect on machining resolution. Int J Mach Tools Manuf 2019;143:92–106.
[13] Belloy E, Thurre S, Walckiers E, Sayah A, Gijs MAM. The introduction of powder blasting for sensor and microsystem applications. Sens Actuators A Phys 2000;84(3):330–7.
[14] Kowsari K, Nouraei H, Samareh B, Papini M, Spelt JK. CFD-aided prediction of the shape of abrasive slurry jet micro-machined channels in sintered ceramics. Ceram Int 2016;42(6):7030–42.
[15] Nouraei H, Wodoslawsky A, Papini M, Spelt JK. Characteristics of abrasive slurry jet micro-machining: a comparison with abrasive air jet micro-machining. J Mater Process Tech 2013;213(10):1711–24.
[16] Matsumura T, Muramatsu T, Fueki S. Abrasive water jet machining of glass with stagnation effect. CIRP Ann Manuf Technol 2011;60(1):355–8.
[17] Zhang XC, Zhou CL, Jiang LY, Guo R. Influence of process parameters on abrasive particle motion characteristics in abrasive water jet descaling. Int J Adv Manuf Technol 2017;90(9–12):2741–9.
[18] Shi LP, Fang Y, Dai QW, Huang W, Wang XL. Surface texturing on SiC by multiphase jet machining with microdiamond abrasives. Mater Manuf Process 2017;33(13):1415–21.
[19] Haghbin N, Ahmadzadeh F, Papini M. Masked micro-channel machining in aluminum alloy and borosilicate glass using abrasive water jet micro-machining. J Manuf Process 2018;35:307–16.
[20] Nouhi A, Lari MRS, Spelt JK, Papini M. Implementation of a shadow mask for direct writing in abrasive jet micro-machining. J Mater Process Technol 2015;223:232–9.
[21] Ghobeity A, Papini M, Spelt JK. Abrasive jet micro-machining of planar areas and transitional slopes in glass using target oscillation. J Mater Process Technol 2009;209(11):5123–32.
[22] Ghobeity A, Krajac T, Burzynski T, Papini M, Spelt JK. Surface evolution models in abrasive jet micromachining. Wear 2008;264(3):185–98.
[23] Wensink H, Elwenspoek MC. Reduction of sidewall inclination and blast lag of powder blasted channels. Sensors Actuators a-Phys 2002;102(1–2):157–64.
[24] Dehnadfar D, Friedman J, Papini M. Laser shadowgraphy measurements of abrasive particle spatial, size and velocity distributions through micro-masks used in abrasive jet micro-machining. J Mater Process Technol 2012;212(1):137–49.
[26] Melentiev R, Fang FZ. Recent advances and challenges of abrasive jet machining. Cirp J Manuf Sci Technol 2018;22:1–20.